CrossMark

ORIGINAL PAPER

Y. G. Miao

On loading ceramic-like materials using split Hopkinson pressure bar

Abstract In Hopkinson pressure bar experiments on ceramics, the stress inequilibrium and indentation of the specimen to bar ends are critical issues due to the brittle nature and high strength of ceramics. Theoretical analysis is employed to reconstruct the loading process for investigating the influence of the stress inequilibrium. The results indicate that it has little influence on the accuracy of stress–strain curves and accurate peak stress measurements during the dynamic test can be made. The optimized bilinear incident wave is formulated for achieving the stress equilibrium and constant strain rate loading on the specimen, and the experimental verification demonstrates the feasibility and merits of the bilinear wave in testing brittle materials. Numerical simulations are also performed to see the effect of bar indentation on stress–strain curves, and simulation results show strain concentration at both ends of the specimens resulting in premature failure. A specimen with a dogbone configuration is proposed which can greatly reduce the strain concentration and facilitate the accurate measurement of stress–strain for brittle materials.

List of symbols

A_s	Cross-sectional area of the specimen
c	Wave speed of material or bar
c_B	Wave speed of the bar
e	Error coefficient
E	Elastic modulus
E_{fitted}	Fitted slope of the calculated stress–strain curves
E_{input}	Input value of the elastic modulus
F	Reflection coefficient
F_{BS}	The reflection coefficient of the stress wave from bar to specimen
F_{SB}	The reflection coefficient of the stress wave from specimen to bar
k	Times of stress wave reverberating between the specimen/bar interfaces

Y. G. Miao (✉)
Joint International Research Laboratory of Impact Dynamics and its Engineering Applications, School of Aeronautics, Northwestern Polytechnical University, Xi'an, Shaanxi 710072, China
E-mail: miaoyinggang@nwpu.edu.cn

Y. G. Miao
Shaanxi Key laboratory of Impact Dynamical and Engineering application, School of Aeronautics, Northwestern Polytechnical University, Xi'an, Shaanxi 710072, China

Y. G. Miao
State Key Laboratory for Strength and Vibration of Mechanical Structures, Department of Engineering Mechanics, School of Aerospace Engineering, Xi'an Jiaotong University, Xi'an, Shaanxi 710049, China

l_s	Length of the specimen
N	Mechanical impedance ratio of bar to specimen
$R(t)$	Stress inequilibrium ratio in the specimen
T	Transmission coefficient
T_BS	The transmission coefficient of the stress wave from bar to specimen
T_SB	The transmission coefficient of the stress wave from specimen to bar
ε_i	The incident strain wave
ε_r	The reflected strain wave
ε_t	The transmitted strain wave
$\varepsilon_\mathrm{true}$	True strain
$\varepsilon_\mathrm{engi.}$	Engineering strain
$\dot{\varepsilon}_\mathrm{d}$	Desired constant strain rate
α	Area ratio of the bar to the specimen
σ_r	Reflected stress wave
σ_i	Transmitted stress wave
$\sigma_\mathrm{I/S}$	Stress at the interface of incident bar/specimen
$\sigma_\mathrm{T/S}$	Stress at the interface of transmitted bar/specimen
σ_true	True stress
$\sigma_\mathrm{engi.}$	Engineering stress
$\triangle l$	Distance if two couples of strain gauges cemented on the bar
τ	Characteristic time of specimen
τ_s	Rise time of stress wave
ρ	The mass density of the bar material

1 Introduction

High-strength ceramics have received extensive interest from the scientific and industrial communities due to their light weight and excellent impact and shock resistance [1,2]. Considering the protection applications being subject to extreme loads induced by explosions and impacts, it is essential to well understand their mechanical behavior and constitutive model under wide strain rate loading, in the hope for improving safety and serviceability of the designed structures [3–7]. It is still challenging for the community of the experimental mechanics to measure the dynamic properties of ceramics [4–10]. The split Hopkinson bar technique (SHPB) is the most classical method for high strain rates testing of materials due to its high level of accuracy. It was originally developed for detecting explosive waves by Hopkinson [8] and developed revolutionarily by Kolsky [4] to test the dynamic mechanical behavior of materials under high strain rates. However, in experimenting with ceramics which present a critical brittle behavior, attention must be paid to accurate measurements. In Refs. [11,12], dynamic mechanical properties and failure processes of ceramics were investigated by using SHPB with the aid of high-speed cameras. The WC platens were used to avoid the potential damage to the bar and reduce the indentation. The images from high-speed cameras also indicated that the failure initiated at both ends of the specimen. Besides, in their experiments, the pulse-shaping techniques were used to trim the incident wave for the stress equilibrium of the specimen [7,11,12]. Therefore, it was found that for ceramics with high strength/elastic modulus and critical embrittlement, the experiments of SHPB need to pay great attention to the following issues. The stress inequilibrium issue is a specific characteristic of the stress wave from SHPB loading, and the indentation is the other potential issue. Within the initial loading process of SHPB, the stress inequilibrium inevitably affects the experimental accuracy level, especially in the initial loading time. Ravichandran et al. [7] suggested that the specimen could achieve the dynamic stress equilibrium after the linear ramp loading wave had reverberated three times in the specimen, and the concept of limiting strain rate was proposed based on the previous findings [6,7]. Their conclusions were drawn that the failure strength data were valid only when the stress state in the specimen was equilibrated (the stress inequilibrium ratio $< 5\%$). However, there was little information about the quantitative evaluation of the stress inequilibrium influence on the measurement accuracy.

Within the process of achieving the stress equilibrium, the accumulated strain could be considered especially for some ceramics with a small failure strain. Thus, more questions need to be answered about the SHPB technique: how to achieve the stress equilibrium state in specimen sooner, how the stress inequilibrium influences the accuracy of stress–strain curves, and how to optimize the incident wave to achieve the loading

of constant strain rate sooner. Yang [13] studied the effect of the specific profile of the incident after analyzing the effect of the rising edge of the incident wave and found that there was an optimum incident wave shape which promotes the attainment of the stress equilibrium sooner. Zhu [14] investigated the stress distribution on concrete-like brittle materials under SHPB loading, and it was found that a different rise time τ_s of incident waves evidently influenced the stress uniformity and that the optimum rise time, either shorter or longer rise time, would result in a worse situation in stress uniformity. About the inertial effect induced by dynamic loading, detailed analyses were conducted to deduce the additional stress in the specimen after considering the inertial effect [4,15–18]. Their results also indicated that loading with a constant strain rate would greatly reduce the inertial effect. But concerning the question: how to achieve constant strain rate loading, the theoretical solution of the incident wave is scarcely treated in the available literature. Fortunately, experimental methods are available. Frew et al. [19] introduced the pulse shaper technique to achieve a constant strain rate loading while testing rock materials by SHPB. Later, they presented an analytical model and data that showed that a wide variety of incident pulses could be produced by varying the geometry of the copper disks and the length and striking velocity of the striker bar [20]. Similar techniques were widely used in the investigations of brittle materials and the small strain measurement [6,11,21,22]. Besides, for the materials whose strengths and failure models are highly rate-dependent, it is more important to achieve a constant strain rate loading for the high-accuracy experiments. The validity of the measurement results was also examined in detail for the obtained stress–strain curves [23,24].

Concerning the indentation effect, it is much pronounced while testing a hard and small diameter specimen [5]. When the stiffness of the specimen is higher than that of the bars of SHPB, severe indentation occurs at both end faces of the bars. It cannot only affect the propagation of the one-dimensional stress wave in SHPB tests but induce the strain concentration on both ends of the specimen as well. The concentration can easily induce the local failure of brittle ceramics too, which could even lead to the fracture of the whole specimen. So, it brings much trouble in the measurement accuracy.

This paper focuses on the accurate dynamical measurement of high strength/elastic modulus ceramics using SHPB. Firstly, the influence of the stress inequilibrium is quantitatively evaluated using the methodology of reconstructing the initial loading process of the stress wave. Then, the incident wave is optimized and the theoretical solution is obtained. The case investigations demonstrate the merits of the optimized loading wave: achieving the stress equilibrium deformation and the loading of the constant strain rate sooner. Finally, the indentation influence is investigated numerically to analyze the potential problems. The influence is elaborately analyzed, and a methodology is proposed for the accurate measurement of the related materials.

2 Influence of the stress inequilibrium

The split Hopkinson bar apparatus is widely used to measure the dynamic mechanical behavior of materials under high strain rates [11–16] since its evolution [4]. The schematic map is shown in Fig. 1.

The strain rate, strain, and stress of the specimen are calculated based on the strain wave signals from the strain gauges cemented on the incident and transmitted bars by using Eq. (1) [9]:

$$\begin{cases} \dot{\varepsilon}_{\text{engi.}} = \frac{c_B}{l_s}(\varepsilon_i - \varepsilon_r - \varepsilon_t), \\ \varepsilon_{\text{engi.}} = \frac{c_B}{l_s}\int_0^t (\varepsilon_i - \varepsilon_r - \varepsilon_t)\mathrm{d}t, \\ \sigma_{\text{engi.}} = \frac{E_B A_B}{2 A_s}(\varepsilon_i + \varepsilon_r + \varepsilon_t), \end{cases} \tag{1}$$

where A, E, and c_B are the cross-sectional area, elastic modulus, and wave speed of the bar, respectively. The propagation velocity of stress wave can be calculated by $c_B = \sqrt{E/\rho}$, where ρ is the mass density of the bar material. l_s and A_s are the length and cross-sectional area of the specimen. ε_i, ε_r, and ε_t are the incident strain wave, the reflected strain wave, and the transmitted strain wave, respectively. With the assumption of a
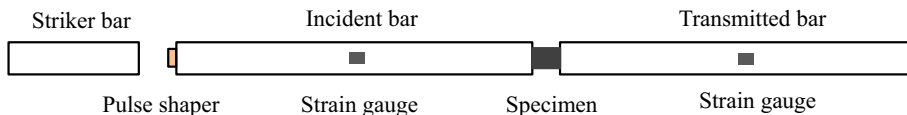

Fig. 1 Schematic diagram of split Hopkinson pressure bar apparatus

constant volume of the specimen while deforming, the true strain $\varepsilon_{\text{true}}$ and true stress σ_{true} are obtained as a function of engineering strain $\varepsilon_{\text{engi.}}$ and engineering stress $\sigma_{\text{engi.}}$ according to Eq. (2) [6].

$$\begin{cases} \varepsilon_{\text{true}} = -\ln(1 - \varepsilon_{\text{engi.}}), \\ \sigma_{\text{true}} = \sigma_{\text{engi.}}(1 - \varepsilon_{\text{engi.}}). \end{cases} \tag{2}$$

2.1 Reconstruction of stress wave loading

The mechanical impedance of the Hopkinson bar or the specimen is defined by $\rho c A$, where ρ, c, and A are the density, wave speed, and sectional area of the bar material, respectively. The characteristic time of the specimen is defined as $\tau = l_s/c_s$, which is the time needed for the stress wave to propagate through the specimen. Figure 2 elaborately shows the reflection and transmission of stress waves at the incident/specimen and the specimen/transmitted bar interfaces. The amounts of the reflected and transmitted waves at the interfaces depend on the mechanical impedance ratio of the bars and the specimen. Based on the one-dimensional stress wave theory, the reflected coefficients F, and transmitted coefficients T are given as follows [25,26]:

$$\begin{cases} T_{\text{BS}} = \frac{2\alpha}{1+n}; & F_{\text{BS}} = \frac{1-n}{1+n}, \\ T_{\text{SB}} = \frac{2n}{n\alpha+\alpha}; & F_{\text{SB}} = \frac{n-1}{n+1}, \end{cases} \tag{3}$$

where T_{BS} is the transmitted coefficient of the stress wave from bar to specimen, and this labeling strategy is also applied to the other coefficients accordingly. n is the mechanical impedance ratio of the bar to the specimen defined by $(\rho c A)_{\text{B}}/(\rho c A)_{\text{S}}$, and $\alpha = A_{\text{B}}/A_{\text{S}}$. In the analysis, we focus on the mechanical behavior of a high-strength ceramic specimen, whose failure strain is lower than 1%. Hence, it is reasonable that the characteristic time of the specimen $\tau = l_s/c_s$ is assumed to be constant during loading. The reflected stress wave σ_r, the transmitted stress wave σ_i, the stress at the interface of incident bar/specimen $\sigma_{\text{I/S}}$, and the stress at the interface of transmitted bar/specimen $\sigma_{\text{T/S}}$ are deduced as follows:

$$\begin{cases} \sigma_r = \sigma_i(t) \cdot F_{\text{BS}} + \sum_1 \sigma_{\text{inc.}}(t - 2k\tau) \cdot T_{\text{BS}} \cdot F_{\text{SB}}^{2k-1} \cdot T_{\text{SB}}, \\ \sigma_{\text{I/S}} = \sigma_i + \sigma_r = \sigma_i(t) + \sigma_i(t) \cdot F_{\text{BS}} + \sum_1 \sigma_{\text{inc.}}(t - 2k\tau) \cdot T_{\text{BS}} \cdot F_{\text{SB}}^{2k-1} \cdot T_{\text{SB}}, \\ \sigma_{\text{T/S}} = \sigma_t = \sigma_i(t - \tau) \cdot T_{\text{BS}} \cdot T_{\text{SB}} + \sum_1 \sigma_i(t - (2k+1)\tau) \cdot T_{\text{BS}} \cdot F_{\text{SB}}^{2k} \cdot T_{\text{SB}}, \end{cases} \tag{4}$$
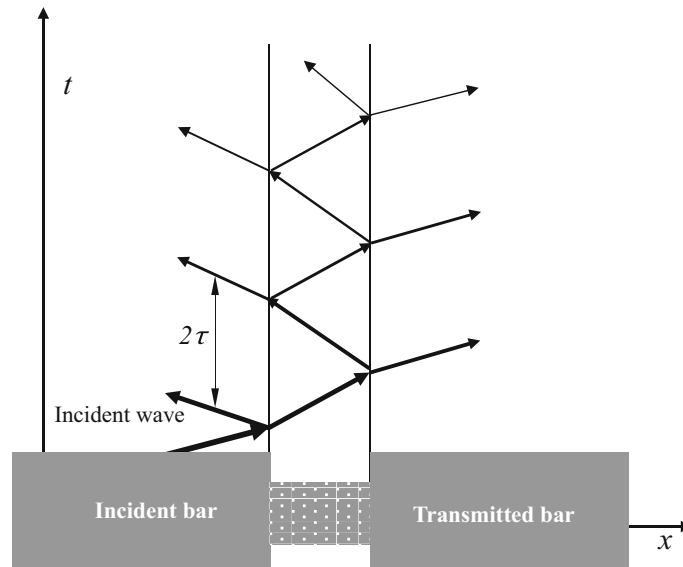
Fig. 2 Reflection and transmission of waves at interfaces of the specimen and bars
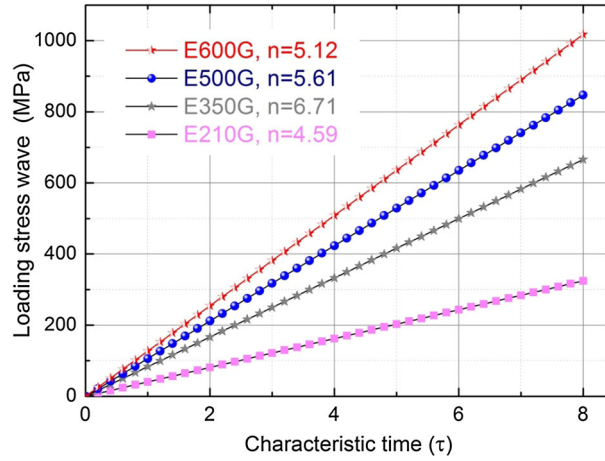
Fig. 3 Loading linear stress waves for different cases

where k is the number of reverberations of the stress wave between the specimen/bars interfaces. The parameter $R(t)$ is used to evaluate the level of the stress inequilibrium in the specimen and is defined as [7]:

$$R(t) = \frac{(\sigma_{I/S} - \sigma_{T/S})}{(\sigma_{I/S} + \sigma_{T/S})/2} \times 100\% \tag{5}$$

The specimen is considered to be in stress equilibrium when $R(t)$ is smaller than 5% [7]. The actual loading history in the sandwiched specimen is thus reproduced, and the stress–strain relations are reconstructed to analyze the influence of the stress inequilibrium on the stress–strain curve.

2.2 Influence analysis

In actual experimenting, the initial loads on the specimen are linear due to a wave propagating characteristics, namely the load is linearly increasing with time increasing loading, no matter with the trapezoidal wave and others [5–7,9,11–14]. Thus, the linear stress waves are selected to conduct the calculation and analysis as shown in Fig. 3 for different cases. The loading slopes are different, aiming to achieve the maximum strain up to around 0.5% within a characteristic time 8τ. The numerical calculations are done on different high-strength ceramic materials. The dimensions and mechanical parameters of the split Hopkinson pressure bars and specimens are listed in Table 1, where the steel bar is adopted, and the case of the steel specimen is also analyzed for reference. The thickness of all specimens is 7 mm. For the high-strength ceramic with a linear elastic behavior, the elastic modulus is the most fundamental parameter, and thus, the reconstructed elastic modulus under the loading of the stress waves is selected to evaluate the influence of the stress inequilibrium.

Figure 4 shows the stress inequilibrium ratio with increasing characteristic time. It is obvious from Fig. 4 that it is inevitable for the specimen to experience severe stress inequilibrium deformation during the initial period of 2τ. The stress inequilibrium ratio $R(t)$ reduces down to below 20% at 2τ. From then, $R(t)$ fluctuates to decrease to 5% after 6τ. The enlarged inset of Fig. 4 shows clearly the difference of the different mechanical impedance from $n = 4.59$ to $n = 6.71$. The stress inequilibrium ratio decreases a little with increasing impedance.

Table 1 Dimensions and mechanical parameters of the Hopkinson bars and the specimen

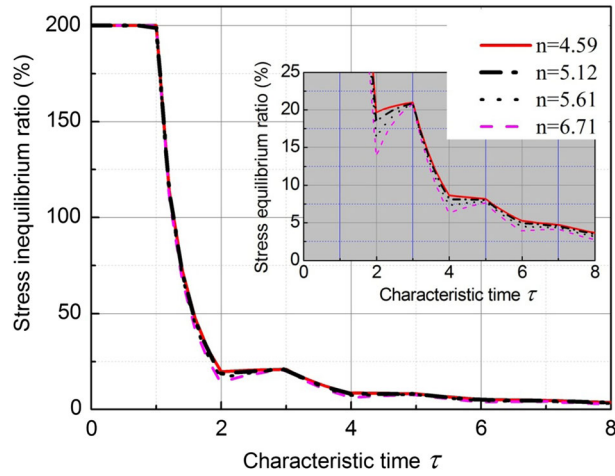|	Diameter (mm)	Elastic modulus (GPa)	Density (kg/m^3)	Wave speed (m/s)	Impedance ratio
Incident/transmitted bar	15	210	7830	5179	1
Specimen E210	7	210	7830	5179	4.59
Specimen E350	7	350	2200	12,613	6.71
Specimen E500	7	500	2200	15,076	5.61
Specimen E600	7	600	2200	16,514	5.12

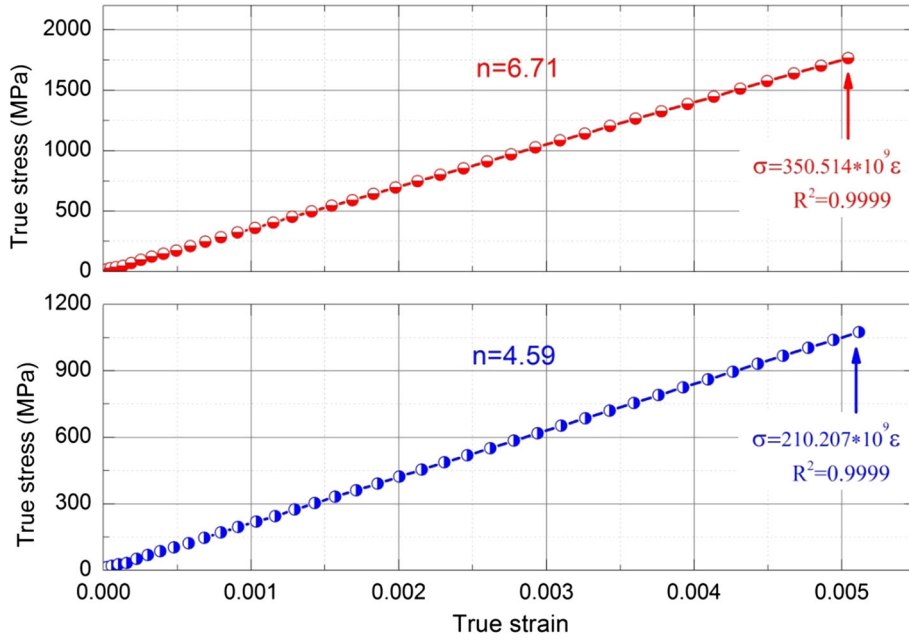**Fig. 4** Stress inequilibrium ratio of specimen under linear ramp loading wave

Fig. 5 Calculated stress–strain curves within characteristic time 8τ

Under a load of this linear stress wave, the loading process is reconstructed based on Eqs. (3) and (4); then, the reflected stress wave and transmitted stress wave are obtained. Those are substituted into Eq. (1) along with the linear incident stress wave, and then the specimen stresses and strains within 8τ are obtained. In the calculation process, the slope of the linear stress wave is adjusted to achieve the maximum strain about 0.5% at 8τ. The stress–strain curves for $n = 6.71$ and 4.59 are displayed in Fig. 5.

The specimen stress–strain curves are linearly fitted to obtain the elastic modulus at each characteristic time, respectively. Error analysis of the elastic modulus is then conducted. The error coefficient is defined by

$$e = \frac{E_{\text{input}} - E_{\text{fitted}}}{E_{\text{input}}} \times 100\%, \tag{6}$$

where E_{fitted} is the fitted slope of the calculated stress–strain curves and E_{input} is the input value of the elastic modulus listed in Table 1. Two error curves for the cases $n = 4.59$ and 6.71 are plotted in Fig. 6. The errors are sharing the same trend: with the loading time increasing, the errors are decreasing from 4% at around 2τ to lower than 1% at 4τ. Even though the ratio at 2τ is about 15%, the corresponding error is lower than 5%. Thus,
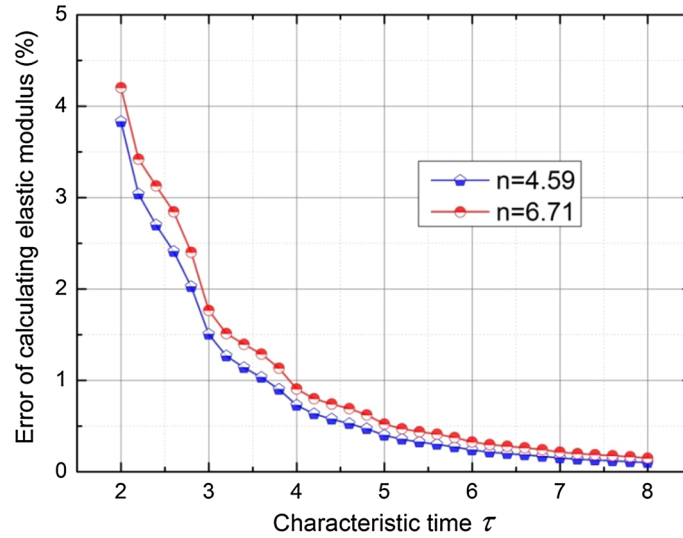
Fig. 6 Error trend with the increase in characteristic time within 8τ

it is concluded that, for the investigated cases, the stress inequilibrium has a small influence on the accurate determination of elastic modulus. Namely, even though the specimen has not achieved the stress equilibrium deformation (the ratio < 5%), the stress–strain curve is still obtained accurately.

3 Bilinear incident waves

For the case of specimen E350 (in Table 1) under a linear ramp loading, the reconstructed stress–strain curve and corresponding strain rate are obtained and plotted in Fig. 7. It is clear that the strain rate is not constantly increasing from 0 to 1643 s^{-1} at strain 0.35%. Under this condition, it is hard to determine how much the loading strain rate is during the specimen's deformation. For materials with mechanical properties sensitive to strain rate, it is necessary to conduct a constant strain rate loading on them for an accurate measurement. Besides, the inconstant strain rate induces severe inertial effect which acts a negative role in the accuracy of the stress–strain curves [4,15–18]. Another problem is how to achieve stress equilibrium loading sooner. As shown in Fig. 6, it is indicated that for one experiment, achieving the stress equilibrium in the specimen much sooner can generate a lower error in determining the elastic modulus. So, it is of great importance to optimize the incident wave to achieve stress equilibrium and the desired constant strain rate loading quicker.

3.1 Optimizing incident wave

In order to achieve stress equilibrium and constant strain rate deformation in the specimen sooner, we propose the following requirements for the optimized incident wave. The first formula aims for achieving the stress equilibrium on the specimen, and the second formula aims for the constant strain rate loading on the specimen:

$$\begin{cases} R(t) = \dfrac{(\sigma_{\mathrm{I/S}} - \sigma_{\mathrm{T/S}})}{(\sigma_{\mathrm{I/S}} + \sigma_{\mathrm{T/S}})/2} \le 0.05, \\ \ddot{\varepsilon}(t) = \dfrac{c_{\mathrm{B}}}{l_{\mathrm{s}}} \left(\dot{\varepsilon}_{\mathrm{i}}(t) - \dot{\varepsilon}_{\mathrm{r}}(t) - \dot{\varepsilon}_{\mathrm{t}}(t) \right) = 0, \\ t \in [2\tau, 6\tau]. \end{cases} \tag{7}$$

As demonstrated in Fig. 4 and Ref. [7], the stress inequilibrium ratio is increasing again after 2τ. It is linked with the continuous loading of this linear stress wave since then. Thus, it would be valid to optimize the slope since this time, aiming for the continuous decrement of the stress inequilibrium. It is found in Fig. 7 that even though the loading strain rate is increasing, the increment is smaller and smaller. Thus, to adjust the slope of
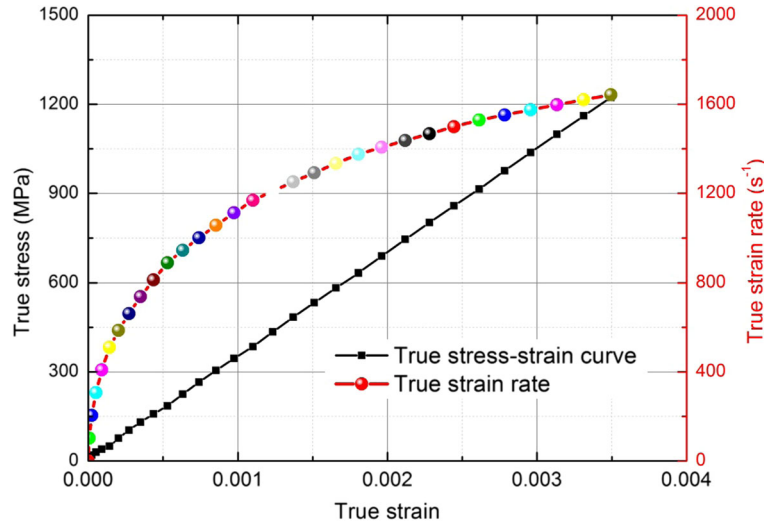
Fig. 7 Reconstructed stress–strain curve and corresponding strain rate under linear loading wave

the loading stress wave could help to achieve a constant strain rate, to meet the second formula of Eqs. (7). In actual experiments, the traditional loading stress waves are usually trapezoidal or triangular profiles, which can be formulated by a series of linear stress waves. Therefore, the slope of the loading stress wave after 2τ is optimized to meet the requirements of Eq. (7). Then, an optimized solution is obtained with a bilinear configuration as Eq. (8), for materials with a linear elastic behavior:

$$\sigma_{\text{inc.}} = \begin{cases} k_1 \cdot t & t \leq 2\tau, \\ 2\tau \cdot k_1 + k_2 \cdot t & t \geq 2\tau, \end{cases} \tag{8}$$

where $k_1 = \frac{\dot{\varepsilon}_d \cdot l_s \cdot E_B}{\tau \cdot c_B \cdot (2 - 2F_{BS} - F_{BS} \cdot T_{BS})}$ and $k_2 = \frac{A_s}{A_B} \cdot \dot{\varepsilon}_d \cdot E_s$ in which $\dot{\varepsilon}_d$ is the desired constant strain rate.

3.2 Cases for some ceramics loading

With the guidance of Eq. (8), the specimen E350 in Table 1 is selected as a case to display the merits of the bilinear wave. In the following analysis, the ceramic specimen with elastic modulus 350 GPa is analyzed under three strain rate loadings, respectively. Figure 8 shows the optimized incident stress waves. It is indicated from the configurations that the slopes of the incident wave change at 2τ. With the increase in the desired strain rate, both slopes of each loading wave increase too. Under these stress waves loadings, the stress inequilibrium ratios of specimen E350 are obtained and shown in Fig. 9. It is found that the three ratio curves are coincident. After 2τ, the ratios continuously drop to 5% at about 4τ (shown in the inset of Fig. 9). The corresponding strain rates under the three bilinear waves are plotted in Fig. 10. The strain rate increases from 0 to the desired strain rates at 2τ, after that the specimen comes into the constant strain rate deformation. The accumulated strain within 2τ increases with the increase in the desired strain rate. When the loading strain rate is high enough, the deformation of the specimen just achieves the failure strain at 2τ. Then, this strain rate should be called *limiting strain rate*. But this *limiting strain rate* is much higher than that of Ref. [7]. This is because Ravichandran et al. evaluated the experimental validity only with the stress inequilibrium ratio 5% and demonstrated that the stress–strain curve was valid after 6τ. So, the *limiting strain rate* in this work should be higher than that of Ravichandran et al. by around three times. Based on the above analysis of the stress inequilibrium (as shown in Fig. 6), the stress–strain curves are still obtained with enough accuracy at the initial loading of 2τ.

3.3 Experiments on a brittle material

In the verification experimenting, the ceramic SiC is originally selected. However, the indentation effect is severe of the SiC specimen to the bar ends and causes more troubles in displaying the merits of the bilinear
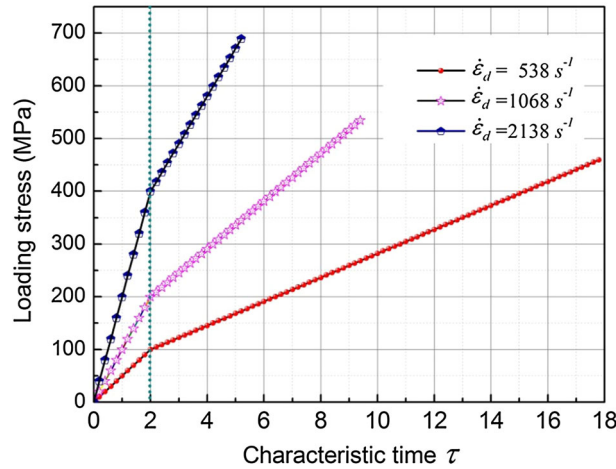
Fig. 8 Optimized bilinear waves for specimen E350 for different strain rates
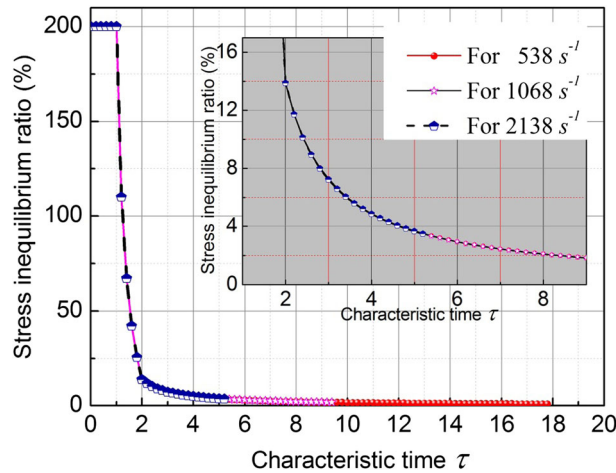

Fig. 9 Stress inequilibrium ratios under the loading of bilinear waves

loading wave. So, the experiment is conducted on a brittle CFRP composite, to verify the experimental feasibility of the proposed bilinear incident wave. The dimensions and mechanical parameters of the Hopkinson bars and CFRP specimen are listed in Table 2.

The pulse shaper technique is employed to trim the incident wave [11,12,19]. The pulse shaper used here is superimposed by an annealed copper pad and a paper scrap to obtain the bilinear loading curve. After adjusting the dimensions of the copper and paper sheets to be Φ 3 mm$\times$ and 1 mm and Φ 2 mm $\times$ 0.2 mm, and the impacting velocity of striker bar 14.7 m/s, a bilinear incident wave can be obtained as shown in Fig. 11, which also includes the reflected and transmitted stress waves. The incident wave has a bilinear configuration in the initial loading section, with the first loading rate slope $S_1 = 7.95 \times 10^6$ MPa/s and the second slope $S_2 = 3.44 \times 10^6$ MPa/s. The duration of the first linear loading part is about 7 μs, which is about twice the normalized time. (τ is about 3.0 μs for this specimen.) The true stress–strain curve is demonstrated in Fig. 12, including the loading characteristics: the corresponding true strain rate curve and the stress inequilibrium ratio curve. The peak on the stress–strain curve indicates the composite fracture initiation, which is usually used as a composite strength. After the peak, stress wave information in Figs. 11 or 12 is inappropriately further analyzed for the mechanical characteristics due to the unknown fracture process.
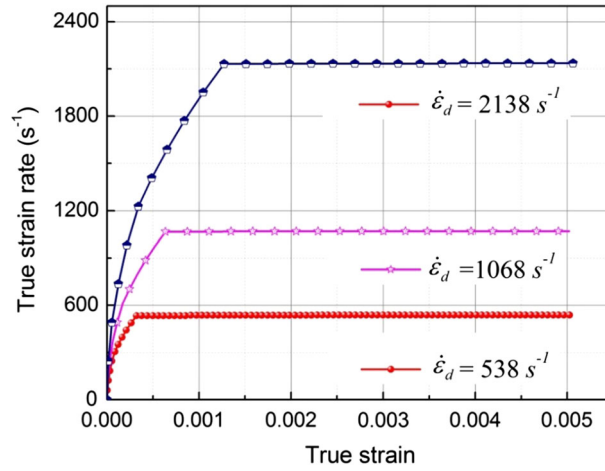
**Fig. 10** True strain rate curves under the loading of bilinear waves

Table 2 Dimensions and mechanical parameters of the Hopkinson bars and CFRP specimen

	Diameter (mm)	Length (mm)	Elastic modulus (GPa)	Density (kg/m^3)	Wave speed (m/s)
Striker bar	15	300	210	7830	5179
Incident bar	15	1500	210	7830	5179
Transmitted bar	15	1500	210	7830	5179
Specimen	11	11	20.3 ± 1.2	1693	NA

The wave speed of the bar is calculated based on the Hopkinson pressure bar verification tests. In the test, two couples of strain gauges are cemented on the bar with the distance $\triangle l$. Then, while the stress wave propagates along the bar, the interval $\triangle t$ is calculated based on the recorded stress waves from the strain gauges. So the wave speed of bar can be obtained. But for the used CFRP specimen, this method does not work due to the dimension limit of the CFRP materials and labeled as NA in this table. The elastic modulus of CFRP is obtained under the loading of strain rate $0.001 \ \mathrm{s}^{-1}$, which is listed here for possible reference
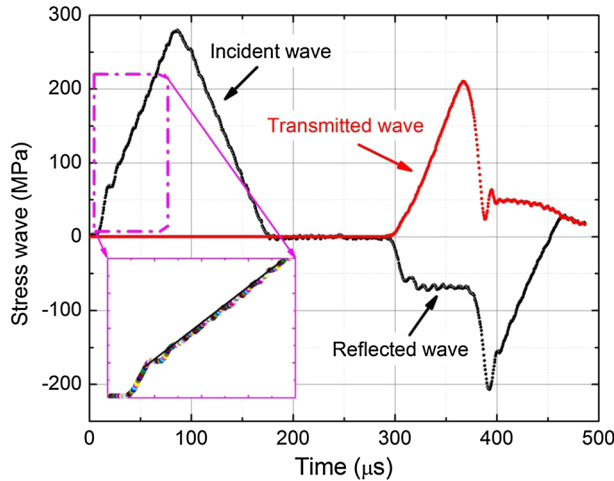
Fig. 11 Bilinear wave loading on CFRP specimen using SHPB
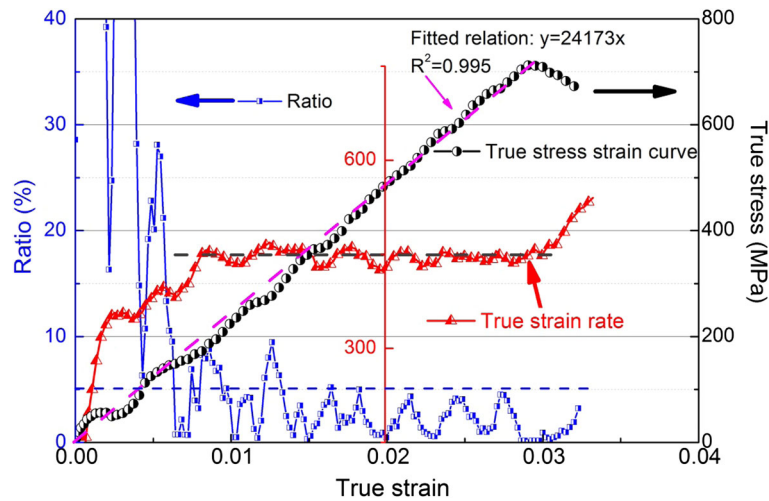
Fig. 12 Stress–strain curve and corresponding loading characteristics under the loading of bilinear wave

4 Indentation influence

Severe indentation occurs at the bar end faces while loading the high-strength specimen. This can not only affect the propagating of one-dimensional stress wave but induce uniform strain distribution on the specimen. Thus, it will affect the experimental results negatively. It is well known that the indentation effect is more pronounced when testing a harder and smaller. diameter specimen [5]. To examine the indentation effect, numerical simulations are conducted to establish the SHPB model by using Abaqus Explicit 6.12 software. In the CAE model, linear elastic mechanical behaviors are assigned to the bars and specimens listed in Table 1. The length of the incident and transmitted bars is 1500 mm. In element controls, hex element shape, sweep technique, and medial axis algorithm are selected. And the intervals and timing in editing field output request are set to be 1200, output at exact times, respectively. Each bar is meshed into at least 80,000 elements, with the type of C3D8R (an 8-node linear brick, reduced integration, hourglass control). Specimens are meshed with at least 600 elements with C3D8R type. The ramp incident wave is applied at the impacting end of the incident bar, with a rising time 65 μs. The normal stresses in the axial direction are output from the middle of the bars for analysis.

The incident wave (as shown in Fig. 13) is applied to the impacting end of the incident bar. The stress S33 in the loading direction is output from the bars or specimen for analysis. Mesh sensitivity analyses are conducted by comparing the results of mesh dimension 1.5 mm and the refined mesh dimension 1 mm. The calculated elastic moduli show less than 0.8% difference after interpreting the simulated data. So, the simulation results with the mesh dimension 1.5 mm are reliable and stable. In the following simulations, the mesh dimensions are controlled to be this size.

4.1 Strain distribution due to indentation

The specimen with the elastic modulus 350 GPa loaded by SHPB is simulated. The specimen details are shown in the row of Specimen E350 in Table 1. When the specimen is loaded by the stress wave for 60 μs, the stress wave has reverberated across the specimen much more than three times, and the stress equilibrium state is assumed to be achieved [7]. So, the results are outputted at this time for further analysis like in Figs. 14, 15, and 16. Figure 14a, shows the sandwiched specimen and the schematic of the normalized distance. When the loading duration is 60 μs, which is much over 8τ, the stress or strain equilibrium of specimen has already been achieved in the specimen in theoretical view as indicated in Fig. 4. But severe deformation occurs on both ends of the specimen. Then, the strain distributions along the loading direction are obtained and shown in Fig. 14b where the strain is normalized by the middle strain of the specimen. It is clearly seen that the strain distribution is not uniform, especially at both ends. The over-strain at both ends is more than the mid strain by 30%. Thus, for the brittle ceramic, both ends come to failure first. Then, the failure at both ends will initiate
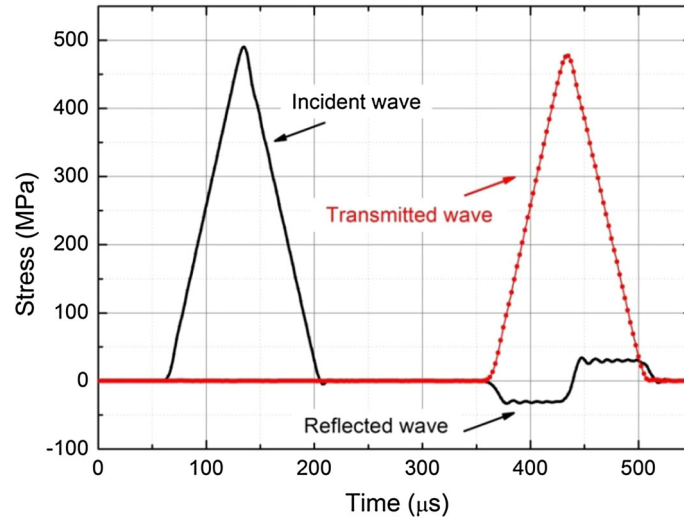
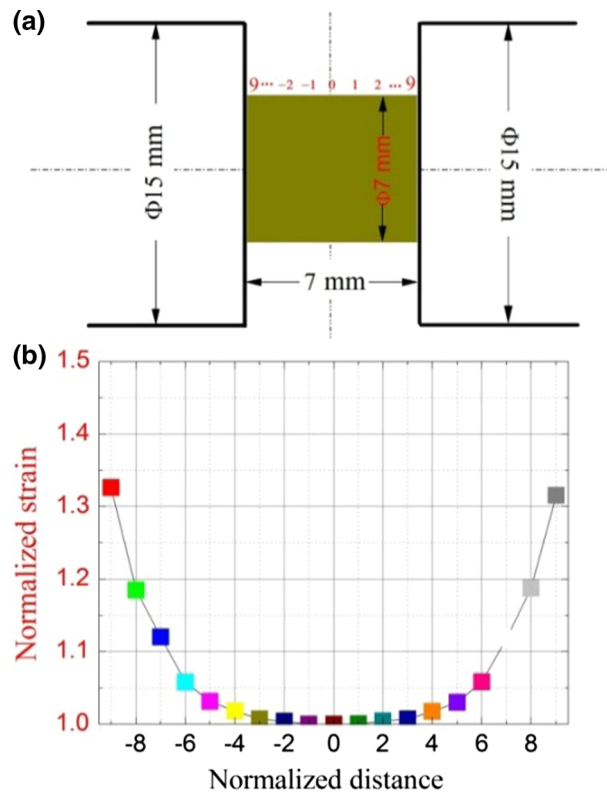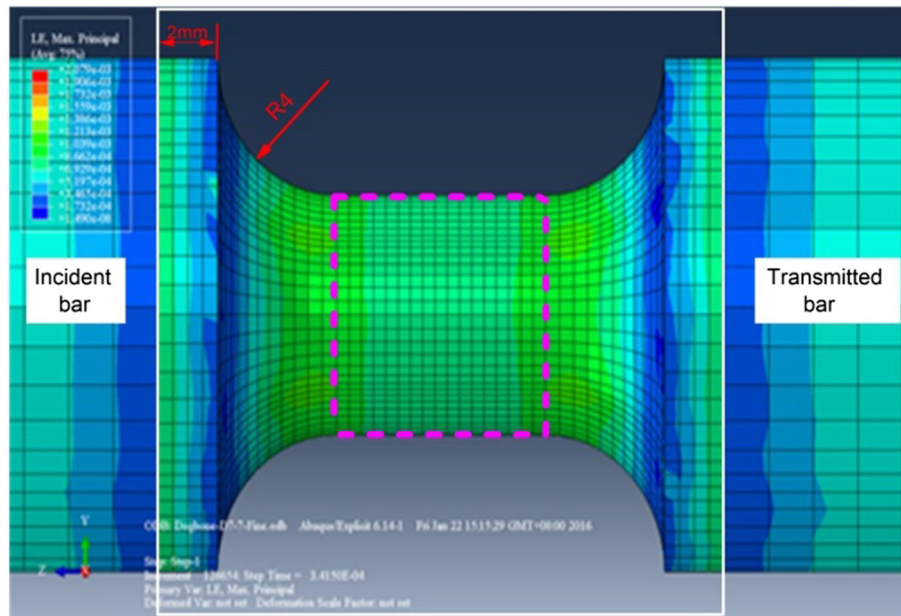**Fig. 13** A group of typical stress waves from numerical simulation

Fig. 14 Strain distributions on the specimen of high-strength ceramic

Fig. 15 Strain contour of dogbone specimen loaded by SHPB

the fracture of the whole brittle ceramics. In the experimental view, this deformation/failure process should be avoided, for the experimented failure strength is lower than their true strength. This also accounts for the fact that the failure occurred at both ends in Refs. [10,11]. In simulating, the ceramic specimen is assumed to behave elastically. Additionally, the simulating results indicate that the maximum strain arrived 0.5% at 8τ. The specimen does not fracture if the failure strain is assumed to be 1% as indicated by Ref. [7].

The strain concentration due to the indentation must affect the propagation of the one-dimensional stress wave at the bar ends and also violates the assumption that the Hopkinson bar end in contact with the specimen remains flat and parallel throughout the experiment [7]. This can not only influence the measurement accuracy of the specimen strength but also affect the strain of specimen obtained from Eq. (1). So, the specific design of specimen configuration should be well considered to ensure a uniform strain distribution in the gauge length. The friction effect is small [27], especially on the deformation of the curves, and not considered in the simulation. Furthermore, in actual experimenting, the friction effect can be reduced to be negligible by adding lubricating oil between the bar ends and the specimen ends.

4.2 Specimen with a dogbone configuration

The specimen with dogbone configuration is introduced and simulated, and the sandwiched section is shown in Fig. 15. The gauge section dimension of the specimen is also $\Phi 7$ mm $\times$ 7 mm, as shown in the dotted line. The bilinear incident wave is also adapted to load the specimen, with the reflected and transmitted wave together as shown in Fig. 13, too. The reflected wave presents a plateau, which means the strain rate of the specimen was constant [4,21]. The strain distribution is also calculated and shown in the bottom of Fig. 16, which is normalized by the middle strain value too. It is clear to find that the strain distribution is rather uniform, and the over-strain at both ends is only 7%. The stress history of specimen ends is calculated based on the simulated incident stress wave, reflected stress wave and transmitted stress wave, and shown in Fig. 17a. It is evident that both stress are well consistent within the loading process. The dogbone specimen presents an abnormal shape, and it must bring some troubles in analyzing the details of stress wave propagating across the abnormal specimen. Thus, the error must exist if the formula of Eq. (1) is still adapted to calculate the stress–strain curves. The results are also calculated as shown in Fig. 17b to demonstrate the error, where the fitted elastic modulus is 137.51 Gpa, which is far lower than the input 350 Gpa. As a reference, the stress and strain of the middle element of the specimen are output and shown in Fig. 17c. The fitted elastic modulus is
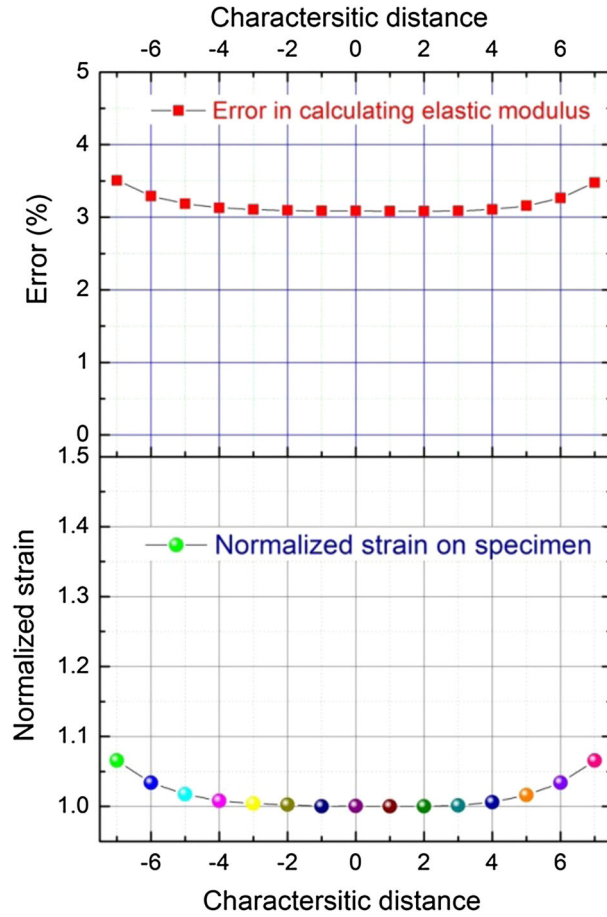
Fig. 16 Strain distributions of dogbone specimen and the error curves in calculating elastic modulus
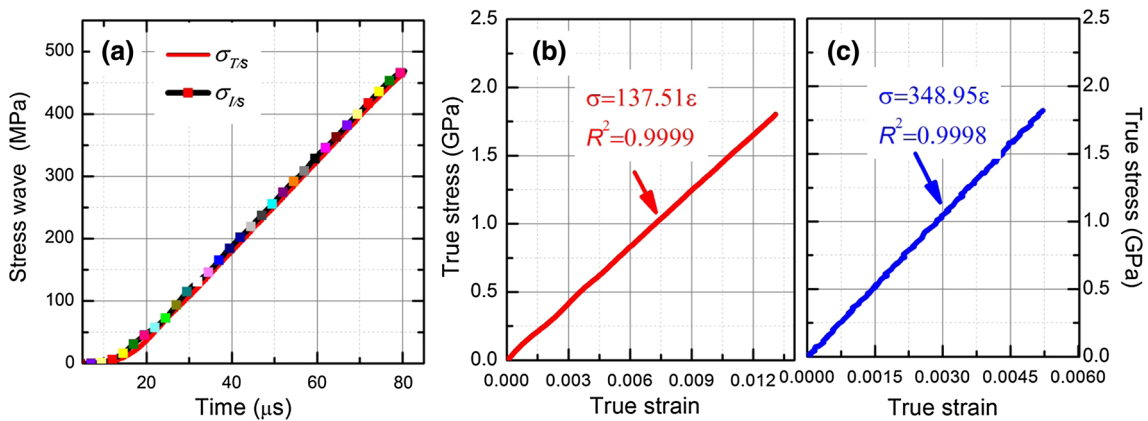

Fig. 17 Stress histories of the specimen and calculated stress–strain curves

approaching to 350 Gpa. Furthermore, it is clearly seen that the calculated strains from Fig. 17b, c are different. The formula result is up to 1.3%, far larger than 0.5% of the middle strain. The deformation of the transition section contributes a lot to the error. So, a methodology is proposed: the strain is obtained from the simulated specimen strain, and the stress is calculated from the transmitted stress. Then, the elastic moduli are fitted, respectively, and plotted in the top of Fig. 16. It is clear that the errors are low enough (lower than 4%). Thus,

the methodology is valid to obtain an accurate interpretation of the data and could be achieved experimentally by cementing the strain gauge to the middle gauge section of the specimen (Fig. 15).

5 Conclusion remarks

To accurately measure the dynamical mechanical properties of ceramics has always been a the hard nut to crack, due to its high strength and critical brittlement. In this paper, theoretical calculations and numerical simulations are adopted to solve the related problems.

Theoretical analysis is employed to reconstruct the initial loading process. The results indicate that the stress inequilibrium ratio $R(t) < 5\%$ is a conservative standard to evaluate the validity of experimental results. After the loading duration over 2τ, the experimental results are valid with the error lower than 5% in view of the reconstructed elastic modulus, even though the stress inequilibrium ratios are still over 15%. Therefore, for the investigated cases of ceramics, the stress inequilibrium has a small influence on the accuracy level of the stress–strain curves. Furthermore, it is also concluded that the accumulated strain within 2τ should be lower than the failure strain of the brittle ceramics specimen, or the accuracy of the stress–strain curve would drop. Therefore, there exists a limiting strain rate for brittle materials. But the limiting strain rate is higher by about three times than that of Ref. [7].

In optimizing the incident wave, the bilinear loading wave is proposed which has two merits: the stress inequilibrium ratio drops continuously to 5% at 4τ; the loading strain rate comes into the desired constant range after 2τ. The actual experiment also demonstrates the feasibility of this bilinear incident wave.

Ceramics produce a severe indentation on the bar ends, which adversely affects the uniform strain distribution of the specimen. Numerical simulations demonstrate that the strain concentration occurs at both ends of the specimen, which could easily result in the failure occurring here. The specimen with a dogbone configuration is introduced, and it is found that the strain distribution is rather uniform. It could greatly reduce the strain concentration and facilitate the accurate measurement of strain. The stress–strain curves based on the strain from the specimen and stress from the transmitted stress could give an accurate measurement, with the errors lower than 4% in view of the reconstructed elastic modulus.

References

1. Sarva, S., Nemat-Nasser, S.: Dynamic compressive strength of silicon carbide under uniaxial compression. Mater. Sci. Eng. A **317**, 140–144 (2001)
2. Wang, L.L., Liang, J., Fang, G.D., Wan, X.Y., Xie, J.B.: Effects of strain rate and temperature on compressive strength and fragment size of ZrB_2–SiC–graphite composites. Ceram. Int. **40**, 5255–5261 (2014)
3. Xiao, Y.C., Sun, Y., Yang, Z.Q., Guo, L.C.: Study of the dynamic mechanical behavior of PBX by Eshelby theory. Acta Mech. **228**, 1993–2003 (2017)
4. Kolsky, H.: An investigation of the mechanical properties of materials at very high rates of loading. Proc. Phys. Soc. B **62**, 676–700 (1949)
5. Nemat-Nasser, S., Isaacs, J.B., Starrett, J.E.: Hopkinson techniques for dynamic recovery experiments. Proc. R. Soc. A **435**, 371–391 (1991)
6. Staehler, J.M., Predebon, W.W., Pletka, B.J., Lankford, J.: Testing of high-strength ceramics with the split Hopkinson pressure bar. J. Am. Ceram. Soc. **76**, 536–538 (1993)
7. Ravichandran, G., Subhash, G.: Critical appraisal of limiting strain rate for compression testing of ceramics in a split Hopkinson pressure bar. J. Am. Ceram. Soc. **77**, 263–267 (1994)
8. Hopkinson, B.: A method of measuring the pressure in the deformation of high explosives or by the impact of bullets. Philos. Trans. R. Soc. **213**, 437–452 (1914)
9. Lindholm, U.S.: Some experiments with the split Hopkinson pressure bar. J. Mech. Phys. Solids **12**, 317–335 (1964)
10. Hou, T.X., Xu, Q., Zhou, J.W.: Size distribution, morphology and fractal characteristics of brittle rock fragmentations by the impact loading effect. Acta Mech. **226**, 3623–3637 (2015)
11. Chen, W., Rajendran, A.M., Song, B., Nie, C.: Dynamic fracture of ceramics in armor applications. J. Am. Ceram. Soc. **90**, 1005–1018 (2007)
12. Acharya, S., Sandip, B., Venkitanarayanan, P., Mukhopadhyay, A.K.: Deformation and failure of alumina under high strain rate compressive loading. Ceram. Int. **41**, 6793–6801 (2015)
13. Yang, L.M., Shim, V.P.M.: An analysis of stress equilibrium uniformity in split Hopkinson bar test specimens. Int. J. Impact Eng. **28**, 129–150 (2005)

14. Zhu, J., Hu, S.S., Wang, L.L.: An analysis of stress uniformity for concrete-like specimens during SHPB tests. Int. J. Impact Eng. **36**, 61–72 (2009)
15. Davies, E.D.H., Hunter, S.C.: The dynamic compression testing of solids by the method of the split Hopkinson pressure bar. J. Mech. Phys. Solids **11**, 155–179 (1963)
16. Samanta, S.K.: Dynamic deformation of aluminium and copper at elevated temperatures. J. Mech. Phys. Solids **19**, 117–135 (1971)
17. Gorham, D.A.: Specimen inertia in high strain-rate compression. J. Phys. Appl. Phys. **22**, 1888–1893 (1989)
18. Song, B., Ge, Y., Chen, W.W., Weerasooriya, T.: Radial inertia effects in Kolsky bar testing of extra-soft specimens. Exp. Mech. **47**, 659–670 (2007)
19. Frew, D.J., Forrestal, M.J., Chen, W.: Pulse shaping techniques for testing brittle materials with a split Hopkinson pressure bar. Exp. Mech. **42**, 93–106 (2002)
20. Frew, D.J., Forrestal, M.J., Chen, W.: Pulse shaping techniques for testing elastic–plastic materials with a split Hopkinson pressure bar. Exp. Mech. **45**, 186–195 (2005)
21. Heard, W.F., Martin, B.E., Nie, X., Slawson, T., Basu, P.K.: Annular pulse shaping technique for large-diameter Kolsky bar experiments on concrete. Exp. Mech. **54**, 1343–1354 (2014)
22. Miao, Y.G., Li, Y.L., Liu, H.Y., et al.: Determination of dynamic elastic modulus of polymeric materials using vertical split Hopkinson pressure bar. Int. J. Mech. Sci. **108–109**, 188–196 (2016)
23. Foster, J.T.: Comments on the validity of test conditions for Kolsky bar testing of elastic-brittle materials. Exp. Mech. **52**, 1559–1563 (2012)
24. Brizard, D., Ronel, S., Jacquelin, E.: Estimating measurement uncertainty on stress–strain curves from SHPB. Exp. Mech. **57**, 735–742 (2017)
25. Wang, L.L.: Foundations of Stress Waves. Elsevier, Amsterdam (2007)
26. Chen, W., Song, B.: Split Hopkinson (Kolsky) Bar Design, Testing and Applications. Springer, New York (2010)
27. Song, B., Chen, W., Montgomery, S.T., Forrestal, M.J.: Mechanical response of an alumina-filled epoxy at various strain rates. J. Compos. Mater. **43**, 1519–1536 (2009)